Theoretical study of thermally activated magnetization switching under microwave assistance: Switching paths and barrier height

H. Suto,[1] K. Kudo,[1] T. Nagasawa,[1] T. Kanao,[1] K. Mizushima,[1] R. Sato,[1] S. Okamoto,[2] N. Kikuchi,[2] and O. Kitakami[2]
[1]*Corporate Research and Development Center, Toshiba Corporation, Komukai-Toshiba-cho 1, Saiwai-ku, Kawasaki 212-8582, Japan*
[2]*Institute of Multidisciplinary Research for Advanced Materials, Tohoku University, Katahira 2-1-1, Aoba-ku, Sendai 980-8577, Japan*
(Received 2 December 2014; revised manuscript received 29 January 2015; published 2 March 2015)

Energy barrier height for magnetization switching is theoretically studied for a system with uniaxial anisotropy in a circularly polarized microwave magnetic field. A formulation of the Landau-Lifshitz-Gilbert equation in a rotating frame introduces an effective energy that includes the effects of both the microwave field and static field. This allows the effective-energy profiles to rigorously describe the switching paths and corresponding barrier height, which govern thermally activated magnetization switching under microwave assistance. We show that fixed points and limit cycles in the rotating frame lead to various switching paths and that under certain conditions, switching becomes a two-step process with an intermediate state.

DOI: 10.1103/PhysRevB.91.094401 PACS number(s): 75.60.Jk, 75.75.Jn, 76.50.+g, 85.70.Kh

I. INTRODUCTION

Magnetization dynamics in a microwave magnetic field has long been studied. The original motivation was provided by a study on ferromagnetic resonance (FMR) in which a ferromagnetic material exhibits an intriguing resonant response to a microwave magnetic field [1,2]. Magnetization switching under this kind of condition, so-called microwave-assisted magnetization switching (MAS) [3], has attained recent attention because of its applications in the field of magnetic recording [4]. The proposed recording technique, microwave-assisted magnetic recording (MAMR), employs a combination of a static field and a microwave field to switch magnetization in a recording medium. Because the magnetization excitation induced by the microwave magnetic field significantly reduces the switching field, MAMR is regarded as a promising method for writing on high-coercivity media material that is likely to be used in future high-density magnetic recording technology. In addition to reducing the switching field, MAS enables selective switching of the magnetization of a specific magnetic body, even when there are several other bodies nearby, because the microwave field frequency (f_{rf}) serves as an additional parameter for controlling the magnetization switching. By correctly tuning f_{rf}, magnetization excitation may occur in only a specific magnetic body, reducing the switching field, and thus selective magnetization switching is realized. This feature is suitable for use in three-dimensional magnetic recording that uses recording media with multiple recording layers to increase the recording density [5–9]. By designing each recording layer to have a different frequency response to a microwave field, layer-selective writing can be realized by means of MAS.

In recent years, researchers have extensively studied MAS both by using various experimental techniques to detect magnetization switching and by employing computational methods. The results of these studies indicate that switching depends on f_{rf}, microwave field amplitude, and the magnetic properties of the material [10–15]. In an attempt to theoretically explain the complex behavior of MAS, the stability of magnetization states before switching at 0 K was studied by using the Landau-Lifshitz-Gilbert (LLG) equation formulated in a rotating frame [15–17]. The rationale of this approach is that the effect of a rotating field can be translated as a fictitious field along the easy axis of the magnetic body when f_{rf} is below a critical frequency and its amplitude is given by $2\pi f_{\mathrm{rf}}/\gamma$ where γ is the gyromagnetic ratio. This fictitious field reduces the switching field according to the Stoner-Wohlfarth model. When f_{rf} exceeds the critical frequency, switching field reduction almost disappears. These theoretical results show qualitative agreement with experimental results, which has allowed the theoretical approach to be widely accepted [15].

The loss of the stability of magnetization states before switching, however, does not always guarantee switching if there exists another stable state on the path to the final switched state [17,18]. In addition, thermal fluctuation causes magnetization switching to occur stochastically at finite temperature, even when the magnetization states before switching are stable and separated by a barrier from the final state. Given these circumstances, it is essential to evaluate the switching paths and the corresponding barrier height in order to better understand MAS including a thermally activated region.

In this paper, we investigate magnetization switching under microwave assistance by introducing an effective energy derived from the LLG equation formulated in a rotating frame. Profiles of the effective energy describe the switching paths and corresponding barrier heights, which are the determinative factors for magnetization switching. Switching paths are classified according to the existence and stability of the following two kinds of characteristic magnetization motion: fixed points in the rotating frame that correspond to a magnetization rotating in synchronization with a microwave field and energetically balanced limit cycles in the rotating frame that correspond to a quasiperiodic magnetization motion. The validity of the theory is confirmed by macrospin simulations.

II. THE LLG EQUATION IN A ROTATING FRAME AND EFFECTIVE ENERGY

Figure 1 schematically depicts the system we consider. It has a uniaxial easy axis with an effective anisotropy field $H_{\mathrm{k}}^{\mathrm{eff}}$ that includes crystal anisotropy and demagnetizing fields. This effective anisotropy field has the following relation with the effective perpendicular anisotropy $K_{\mathrm{u}}^{\mathrm{eff}}$

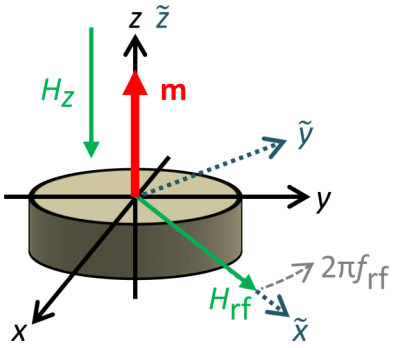

FIG. 1. (Color online) Schematic configuration of the system, initial magnetization direction, and applied magnetic fields. Two sets of coordinates, (x, y, z) and $(\tilde{x}, \tilde{y}, \tilde{z})$, represent the laboratory frame and rotating frame, respectively.

and the saturation magnetization M_s: $H_k^{eff} = 2K_u^{eff}/M_s$. The magnetization direction is denoted by a unit vector $\mathbf{m}$. We assume the axis of symmetry to be the z axis and the initial magnetization direction to be the $+z$ direction. We apply a static field along the $-z$ direction with amplitude H_z and a microwave field rotating counterclockwise in the x-y plane at a frequency of f_{rf} with amplitude H_{rf}. The effective field is therefore expressed as $\mathbf{H}^{eff} = H_{rf}\cos(2\pi f_{rf}t)\mathbf{e}_x + H_{rf}\sin(2\pi f_{rf}t)\mathbf{e}_y + (-H_z + H_k^{eff}m_z)\mathbf{e}_z$. We evaluate switching of the magnetization in these magnetic fields by using the LLG equation $d\mathbf{m}/dt = -\gamma(\mathbf{m}\times\mathbf{H}^{eff}) + \alpha\mathbf{m}\times(\mathrm{d}\mathbf{m}/dt)$, where α denotes the Gilbert damping constant. We normalize time in units of $(\gamma H_k^{eff})^{-1}$ and the magnetic fields in units of H_k^{eff}. The time thus becomes $\tau = t(\gamma H_k^{eff})$, and the effective field becomes $\mathbf{h}^{eff} = h_{rf}\cos(\omega_{rf}\tau)\mathbf{e}_x + h_{rf}\sin(\omega_{rf}\tau)\mathbf{e}_y + (-h_z + m_z)\mathbf{e}_z$, where $h_z = H_z/H_k^{eff}$, $h_{rf} = H_{rf}/H_k^{eff}$, and $\omega_{rf} = (2\pi f_{rf})/(\gamma H_k^{eff})$. When the normalized microwave frequency equals 1 ($\omega_{rf} = 1$), the microwave field frequency coincides with the intrinsic FMR frequency of the system at $h_z = 0$. After this normalization, the magnetization dynamics is described by the following LLG equation:

$$\frac{d\mathbf{m}}{d\tau} = -\mathbf{m}\times\mathbf{h}^{eff} + \alpha\mathbf{m}\times\frac{d\mathbf{m}}{d\tau}. \tag{1}$$

This expression of the LLG equation clearly indicates that the magnetization dynamics can be characterized by the control parameters h_z, h_{rf}, and ω_{rf}. Bertotti *et al.* showed that such magnetization dynamics can be conveniently treated by introducing a rotating frame $(\tilde{x}, \tilde{y}, \tilde{z})$ that shares the symmetrical axis with the laboratory frame ($\tilde{z} = z$) and rotates around the z axis at the frequency of f_{rf} [16]. By this coordinate transformation, the microwave field becomes a static field. We assume the direction of the microwave field to be in the $\tilde{x}$ direction, and consequently the effective field in the rotating frame is expressed by $\tilde{\mathbf{h}}^{eff} = h_{rf}\mathbf{e}_{\tilde{x}} + (-h_z + m_{\tilde{z}})\mathbf{e}_{\tilde{z}}$.

The dynamics of the magnetization in the rotating frame $\tilde{\mathbf{m}}$ is governed by the following LLG equation formulated in the rotating frame:

$$\frac{d\tilde{\mathbf{m}}}{d\tau} = -\tilde{\mathbf{m}}\times(\tilde{\mathbf{h}}^{eff} - \omega_{rf}\mathbf{e}_{\tilde{z}} + \alpha\omega_{rf}\tilde{\mathbf{m}}\times\mathbf{e}_{\tilde{z}}) + \alpha\tilde{\mathbf{m}}\times\frac{d\tilde{\mathbf{m}}}{d\tau}. \tag{2}$$

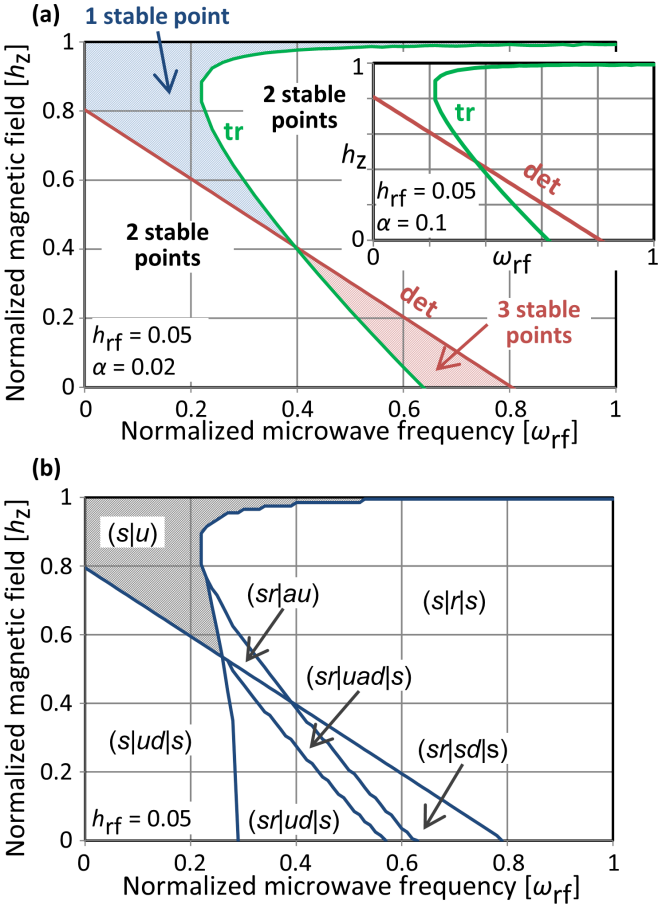

FIG. 2. (Color online) (a) Phase diagram of a system with different numbers of stable fixed points obtained from the approach based on $\det\mathbf{A}$ and $\mathrm{tr}\,\mathbf{A}$. Parameter values are $h_{rf} = 0.05$ and $\alpha = 0.02$. Results for $h_{rf} = 0.05$ and $\alpha = 0.1$ are shown in the inset. (b) Corresponding phase diagram of the phase portrait obtained from the effective-energy approach in the present study.

Next, we briefly explain a previous approach for predicting the switching condition that uses Eq. (2) to evaluate the stability of the magnetization states before switching. First, the fixed points in the rotating frame are obtained by setting $d\tilde{\mathbf{m}}/d\tau = 0$. Equation (2) is then linearized with a small perturbation $\delta\tilde{\mathbf{m}}$ in the tangential plane around the fixed points, which yields the following equation of motion: $(d/d\tau)\delta\tilde{\mathbf{m}} = \mathbf{A}\delta\tilde{\mathbf{m}}$. The stability of the fixed points can be determined by examining the determinant and trace of the matrix $\mathbf{A}$ [15–17]. Figure 2(a) shows a phase diagram of the system with different numbers of stable fixed points in the ω_{rf}-h_z plane for parameter values of $h_{rf} = 0.05$ and $\alpha = 0.02$. There are four regions in the diagram, separated by the boundary obtained from the determinant and the trace. In each region, the system has up to three stable fixed points. We note that this phase diagram does not change drastically for $\alpha = 0.1$, as can be seen from the inset. The region with only one stable fixed point has been interpreted as a switching condition because this stable fixed point corresponds to the final switched state and the magnetization state before switching is unstable. From the shape of the region, it can be seen that the switching field of MAS is expected to decrease linearly as f_{rf} increases and then

to increase suddenly at $\omega_{\rm rf} = 0.4$, which is the intersection of the two boundaries obtained from the determinant and the trace. This $\omega_{\rm rf}$ dependence of the switching field shows qualitative agreement with the experimental results [15]. The frequency at which switching field reduction disappears is referred to as the critical frequency.

As already discussed, this type of evaluation based on the stability of the magnetization states before switching offers insufficient understanding of magnetization switching because another stable state other than a fixed point on the path to the final switched state may exist and prevent switching. To address this problem, we introduce an effective energy that represents the potential of the magnetization direction along switching paths. To begin with, we derive the Landau-Lifshitz form of Eq. (2),

$$\frac{d\tilde{\mathbf{m}}}{d\tau} = -\tilde{\mathbf{m}} \times (\tilde{\mathbf{h}}^{\rm eff} - \omega_{\rm rf}\mathbf{e}_{\tilde{z}}) - \alpha\tilde{\mathbf{m}} \times (\tilde{\mathbf{m}} \times \tilde{\mathbf{h}}^{\rm eff}). \quad (3)$$

In this transformation, higher terms of α are neglected because the condition $\alpha \ll 1$ is satisfied in conventional ferromagnetic materials. Note that the fictitious field $-\omega_{\rm rf}\mathbf{e}_{\tilde{z}}$ in the precessional part that originates from the microwave field acts to promote magnetization switching. We introduce a potential function $\tilde{g}$ from the field term in the precessional part of Eq. (3) and choose this function so as to satisfy $\partial\tilde{g}/\partial\tilde{\mathbf{m}} = \tilde{\mathbf{h}}^{\rm eff} - \omega_{\rm rf}\mathbf{e}_{\tilde{z}}$. When no damping exists (i.e.,$\alpha = 0$), $\tilde{g}$ represents the quantity conserved during magnetization motion, and the magnetization trajectories trace a constant-energy closed contour $C(\tilde{g}_0)$ along which $\tilde{g} = \tilde{g}_0$. Depending on h_z, $h_{\rm rf}$, and $\omega_{\rm rf}$, the condition $\partial\tilde{g}/\partial\tilde{\mathbf{m}} = 0$ has either two or four solutions. For two solutions, they are a maximum and a minimum point of $\tilde{g}$. For four solutions, they are a maximum, a global minimum, a local minimum, and a saddle point of $\tilde{g}$. When the magnetization direction is at these points, it does not move because the right-hand side of Eq. (3) becomes zero. Thus, we refer to these points as fixed points, which are equivalent to the fixed points discussed in the previous approach. When α exists but is small, magnetization trajectories deviate very little from $C(\tilde{g}_0)$ within the time scale of one precession period. Hereafter, we assume that this small-α approximation is valid.

Now, we rewrite Eq. (3) such that the field term of the damping part coincides with that of the precession part, as follows:

$$\frac{d\tilde{\mathbf{m}}}{d\tau} = -\tilde{\mathbf{m}} \times (\tilde{\mathbf{h}}^{\rm eff} - \omega_{\rm rf}\mathbf{e}_{\tilde{z}}) - \alpha\tilde{\mathbf{m}} \times (\tilde{\mathbf{m}} \times (\tilde{\mathbf{h}}^{\rm eff} - \omega_{\rm rf}\mathbf{e}_{\tilde{z}})) - \alpha\omega_{\rm rf}\tilde{\mathbf{m}} \times (\tilde{\mathbf{m}} \times \mathbf{e}_{\tilde{z}}). \quad (4)$$

This yields a third term on the right-hand side that has a form similar to the spin-torque term [18–20]. We can therefore apply the derivation of the effective energy in spin-torque switching [21] to the case of MAS and define the effective energy as

$$\varepsilon(\tilde{g}) = \int_{\tilde{g}_{\rm ref}}^{\tilde{g}} \frac{M(\tilde{g}')}{\mathcal{M}(\tilde{g}')} d\tilde{g}'. \quad (5)$$

This value represents the normalized energy necessary for the magnetization to move from one reference constant-energy contour $C(\tilde{g}_{\rm ref})$ to another contour $C(\tilde{g})$ in the presence of a microwave field. Because of the continuous nature of ε, $\tilde{g}_{\rm ref}$ can take any value of $\tilde{g}$, and we thus set $\tilde{g}_{\rm ref}$ to the maximum value of $\tilde{g}$. Herewith, $\varepsilon(\tilde{g})$ serves as the energy potential of the magnetization in $C(\tilde{g})$. The functions $M(\tilde{g}_0)$ and $\mathcal{M}(\tilde{g}_0)$ are the line integrals $M(\tilde{g}_0) = -\oint_{C(\tilde{g}_0)} (\tilde{\mathbf{m}} \times \tilde{\mathbf{h}}^{\rm eff}) \cdot d\tilde{\mathbf{m}}$ and $\mathcal{M}(\tilde{g}_0) = -\oint_{C(\tilde{g}_0)} (\tilde{\mathbf{m}} \times (\tilde{\mathbf{h}}^{\rm eff} - \omega_{\rm rf}\mathbf{e}_{\tilde{z}})) \cdot d\tilde{\mathbf{m}}$, respectively. The former line integral is proportional to the change in $\tilde{g}$ induced by one precession motion along $C(\tilde{g}_0)$. The actual change in $\tilde{g}$ is given by $-\alpha M(\tilde{g}_0)$. If the third term of Eq. (4) is omitted, the change in $\tilde{g}$ is then given by the following expression using the latter line integral: $-\alpha\mathcal{M}(\tilde{g}_0)$. The two functions, $\tilde{g}$ and ε, are both potential functions, but they are different in that the former reflects only the fictitious field $-\omega_{\rm rf}\mathbf{e}_{\tilde{z}}$ in the precessional part of Eq. (4), whereas the latter reflects both the fictitious field and the third term of Eq. (4). In other words, ε includes all the effects that originate from the microwave field. Because the third term of Eq. (4) mostly acts to prevent magnetization switching, $M(\tilde{g}_0)$ can take zero or negative values, whereas $\mathcal{M}(\tilde{g}_0)$ is always positive. When the condition $M(\tilde{g}_0) = 0$ (i.e., $d\varepsilon/d\tilde{g}|_{\tilde{g}=\tilde{g}_0} = 0$) holds, precession motion along $C(\tilde{g}_0)$ does not change $\tilde{g}$. This means that the trajectory $C(\tilde{g}_0)$ is energetically balanced and represents a limit cycle along which the magnetization continues to precess. Limit cycles can be either attractive (stable) or repulsive (unstable), depending on the shape of the ε profile. Switching paths are determined according to the existence and stability of the fixed points and limit cycles.

Furthermore, ε profile can provide the barrier height for thermally activated magnetization switching. At finite temperatures, the switching rate is governed by the barrier height and thermal fluctuations. The thermal fluctuations are equivalent to a random field $\mathbf{H}^{\rm th}$ that has the Gaussian noise properties and has components in the laboratory frame $H_a^{\rm th}$ $(a = x, y, z)$ that satisfy the following equations [22]:

$$\left\langle H_a^{\rm th}(t) \right\rangle = 0 \quad (6)$$

and

$$\left\langle H_a^{\rm th}(t) H_b^{\rm th}(t') \right\rangle = \mu\delta_{ab}\delta(t - t'), \quad (7)$$

where $\mu = 2\alpha K_{\rm B}T/\gamma M_{\rm s}V$, $K_{\rm B}$ is the Boltzmann constant, and V denotes the volume of a magnetic body. These noise properties are maintained even when the random field is defined in the rotating frame. This is proved by rewriting Eqs. (6) and (7) in the rotating frame, which yields the following equations: $\langle H_{\tilde{a}}^{\rm th}(t)\rangle = 0$ and $\langle H_{\tilde{a}}^{\rm th}(t) H_{\tilde{b}}^{\rm th}(t')\rangle = \mu\delta_{\tilde{a}\tilde{b}}\delta(t - t')$ $(\tilde{a}, \tilde{b} = \tilde{x}, \tilde{y}, \tilde{z})$. Because the noise properties are the same regardless of the chosen frame, the effective energy of MAS defined in the rotating frame can be used in discussing the barrier height for thermally activated magnetization switching. The effective-energy barrier height has the following relation with the actual energy barrier height ΔE: $\Delta E = 2VK_{\rm u}^{\rm eff}\Delta\varepsilon$.

III. MAGNETIZATION SWITCHING UNDER MICROWAVE ASSISTANCE

A. Phase portraits and switching paths

Figure 3 shows various phase portraits that appear depending on h_z, $h_{\rm rf}$, and $\omega_{\rm rf}$. First, we show a bistable system without limit cycles. In Fig. 3(a), four fixed points—corresponding to a maximum, a global minimum, a local minimum, and a saddle point of $\tilde{g}$—and the constant-energy contour of the saddle point are plotted on a plane of the rotating polar coordinates (θ-ϕ) that represent the magnetization direction

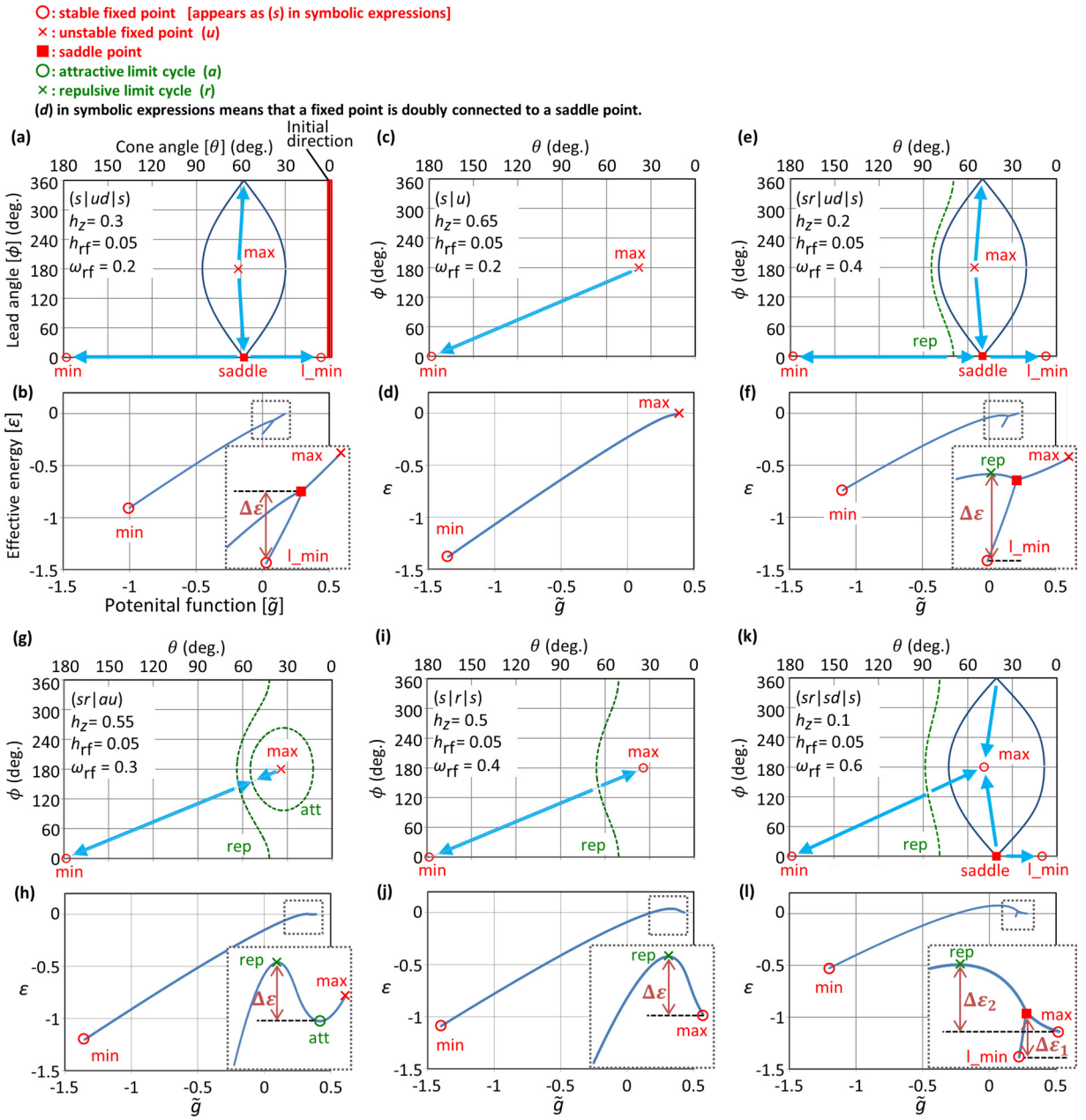

FIG. 3. (Color online) (a) Four fixed points: a maximum, a global minimum, a local minimum, and a saddle point presented in the rotating polar coordinates (θ, ϕ) of the magnetization direction for the phase portrait $(s\,|ud|\,s)$. The stability of each fixed point is represented by either an open circle (stable) or a cross (unstable) except for the saddle point represented by a filled box. The constant-energy contour of the saddle point is shown as a solid line. Arrows show the downward direction of the effective energy on each path connecting the fixed points. The initial magnetization direction along the $+z$ direction corresponds to the right side of the figure ($\theta = 0^\circ$). (b) Corresponding effective energy ε profile plotted versus $\tilde{g}$. The prior notation for the stability of the fixed points is used. Barrier height is represented by $\Delta\varepsilon$. (c) Two fixed points, maximum and minimum points, for the phase portrait $(s|u)$. (d) Corresponding ε profile. (e) Four fixed points and a repulsive limit cycle (a dashed line) for the phase portrait $(sr\,|ud|\,s)$. (f) Corresponding ε profile. A cross denotes the repulsive limit cycle. (g) Two fixed points, a repulsive limit cycle, and an attractive limit cycle, for the phase portrait $(sr|au)$. (h) Corresponding ε profile. An open circle denotes the attractive limit cycle. (i) Two fixed points and a repulsive limit cycle for the phase portrait $(s\,|r|\,s)$. (j) Corresponding ε profile. (k) Four fixed points and a repulsive limit cycle for the phase portrait $(sr\,|sd|\,s)$. (l) Corresponding ε profile.

where θ is the cone angle, and ϕ is the lead angle with respect to the microwave field. Parameters are $h_z = 0.3$, $h_{\rm rf} = 0.05$, and $\omega_{\rm rf} = 0.2$. These values are also shown in the figure. Figure 3(b) shows the corresponding ε profile plotted versus $\tilde{g}$. Because we set $\tilde{g}_{\rm ref}$ in Eq. (5) to the maximum of $\tilde{g}$, the right ends of the profiles always match $\varepsilon = 0$. The stability of the fixed points can be evaluated from this ε profile. The maximum point is unstable, and the global minimum and local minimum points are stable. Saddle points are always unstable. According to these results, the magnetization that initially points in the $+z$ direction ($\theta = 0^\circ$) falls to the local minimum point and oscillates in synchronization with the

microwave field. Because the lead angle is zero ($\phi = 0^\circ$) at the local minimum point, the direction of the microwave field and the magnetization direction are parallel when projected onto the x-y plane (in-phase oscillation). For magnetization switching, it is necessary to overcome the saddle point, and the effective-energy barrier height $\Delta\varepsilon$ for this switching is given by the difference in the effective energy between the local minimum and the saddle point. This phase portrait is represented by $(s\,|ud|\,s)$. The first symbol indicates the stability of the global minimum point and can be either stable (s) or unstable (u). The second symbol indicates the stability of the maximum point. The letter d in this symbol means that this fixed point is doubly connected to the saddle point, as shown in Fig. 3(a), where the two arrows connecting the maximum and saddle points head toward the positive and negative ϕ direction, respectively. The last symbol indicates the stability of the local minimum point.

Deterministic switching occurs when there is neither a stable fixed point nor an attractive limit cycle other than the stable switched state. Figures 3(c) and 3(d) show the results of identical analysis using another set of parameters that satisfies this condition for deterministic switching. Different from the previous $(s\,|ud|\,s)$ phase portrait, the system has two fixed points corresponding to maximum and minimum points of $\tilde{g}$. From the monotonic ε profile, it is clear that the initial magnetization falls straight to the switched state without any barrier. This phase portrait is represented by $(s|u)$, where these two symbols indicate the stability of the minimum and the maximum point in this order.

The previous two phase portraits contain no limit cycles, and the two potential functions $\tilde{g}$ and ε have a monotonic relation. This means that the difference between $\tilde{g}$ and ε does not affect the switching behavior at 0 K, and the condition for such switching can be determined solely by $\tilde{g}$ in which the microwave field is treated simply as the fictitious field along the $-z$ direction with an amplitude of $\omega_{\rm rf}$. Therefore, the boundary between the $(s\,|ud|\,s)$ and $(s|u)$ phase portraits is derived from the Stoner-Wohlfarth model that considers two static magnetic fields: along an in-plane direction with an amplitude of $h_{\rm rf}$ and along the $-z$ direction with an amplitude of $h_z + \omega_{\rm rf}$. This interpretation based on the Stoner-Wohlfarth model is naturally valid at $\omega_{\rm rf} = 0$, where all the applied fields become static and the fictitious field disappears. This fact is reflected in the phase diagram of the phase portraits plotted in the $\omega_{\rm rf}$-h_z plane [Fig. 2(b)], in which the boundary between the $(s\,|ud|\,s)$ and $(s|u)$ phase portraits exists from $\omega_{\rm rf} = 0$ up to the critical frequency. Above the critical frequency, one needs to take limit cycles into account, which we discuss next.

When $\omega_{\rm rf}$ is increased, limit cycles appear, and they play an important role in determining switching paths, as seen in the phase portrait analyzed in Figs. 3(e) and 3(f). This system has four fixed points, just as the $(s\,|ud|\,s)$ phase portrait does. The profile of ε, however, indicates the existence of a repulsive limit cycle in the path from the saddle to the global minimum point. The initial magnetization falls to the local minimum point and oscillates in-phase with the microwave field. For switching it needs to overcome the repulsive limit cycle. This phase portrait is represented by $(sr\,|ud|\,s)$ where the first symbol sr means that the stable global minimum point is surrounded by the repulsive limit cycle (r).

In the phase portrait analyzed in Figs. 3(g) and 3(h), the system has two fixed points, and the profile of ε indicates the existence of an attractive limit cycle and a repulsive limit cycle in the path from the unstable maximum to the stable minimum point. The initial magnetization falls to the attractive limit cycle and shows periodic magnetization motion along the limit cycle path in the rotating frame. Because the period of this limit cycle motion and the period of the rotating microwave field are independent, this magnetization motion becomes quasiperiodic in the laboratory frame. The repulsive limit cycle serves as the barrier to prevent switching. This phase portrait is represented by $(sr|au)$, where the second symbol au means that the unstable maximum point is surrounded by the attractive limit cycle (a).

Figures 3(i) and 3(j) show a phase portrait of a system with two fixed points, which is characterized by the fact that both maximum and minimum points are stable and separated by a repulsive limit cycle. The initial magnetization falls to the maximum point and oscillates in antiphase with the microwave field because $\phi = 180^\circ$ at the maximum point. This phase portrait is symmetric in that the repulsive limit cycle equally surrounds the two stable fixed points. This phase portrait is represented by $(s\,|r|\,s)$.

Interestingly, there are conditions under which switching becomes a two-step process with an intermediate state, as shown in Figs. 3(k) and 3(l). The initial magnetization falls to the local minimum point and needs to overcome the repulsive limit cycle in the path from the saddle to the global minimum point for switching. Other than that, switching can take advantage of the stable maximum point, which makes the switching a two-step process and lowers the individual barrier height of each transition. The first transition needs to overcome the saddle point to reach the stable maximum point, and the second transition needs to overcome the repulsive limit cycle for switching. This phase portrait is represented by $(sr\,|sd|\,s)$. By slightly changing parameters, another phase portrait, $(sr\,|uad|\,s)$ appears, in which an attractive limit cycle surrounds the maximum point and the maximum point becomes unstable. Since the difference between these two phase portraits is the same as that between $(sr|au)$ and $(s\,|r|\,s)$, figures explaining the $(sr\,|uad|\,s)$ phase portrait are not shown. In the $(sr\,|uad|\,s)$ phase portrait, the switching path consists of two transitions and the attractive limit cycle serves as the intermediate state.

Figure 2(b) shows the complete phase diagram of phase portraits for $h_{\rm rf} = 0.05$. The number of letters s in each symbolic expression corresponds to the number of stable fixed points. In this regard, the phase diagram shows exact agreement with the conclusion obtained from the previous approach [Fig. 2(a)], which finds the number of stable fixed points. Because our approach provides a more detailed phase diagram, it can be seen that the region with only one stable fixed point actually consists of $(s|u)$ and $(sr|au)$, and in the latter phase portrait, deterministic switching does not occur. The switching conditions derived from the two approaches, the monostable region in Fig. 2(a) and the $(s|u)$ region in Fig. 2(b), share the tendency that the switching field linearly decreases as $\omega_{\rm rf}$ increases, and suddenly increases. The previous approach, however, overestimates the critical frequency at which the sudden increase in the switching field occurs.

Because we neglect higher terms of α in the derivation of Eq. (3), the phase diagram shown in Fig. 2(b) does not depend on α. In contrast, the previous approach takes α into account in the calculation of the determinant and trace. The boundaries obtained from the determinant and trace, however, differ very little between $\alpha = 0.02$ and $\alpha = 0.1$ [Fig. 2(a) and inset]. This fact suggests that our approach is also valid for values of α in this range, which covers most of the conventional ferromagnetic materials.

B. Barrier height for magnetization switching

In the previous section, we showed that our approach to MAS through utilizing an effective energy can treat switching paths including fixed points and limit cycles. Furthermore, the approach enables us to calculate the barrier height $\Delta\varepsilon$ by considering the variety of equilibrium states before switching and the barrier states. Figure 4(a) shows $\Delta\varepsilon$ as a color map in the $\omega_{\rm rf}$-h_z plane. The microwave field amplitude $h_{\rm rf}$ is set to 0.05. The black region corresponds to $(s|u)$, where no barrier exists. For the phase portraits $(sr\,|sd|\,s)$ and $(sr\,|uad|\,s)$, where switching consists of two transitions, only the higher of the two barrier heights is plotted. As $\omega_{\rm rf}$ increases from zero up to the critical frequency around $\omega_{\rm rf} = 0.25$, the $(s|u)$ region grows toward the lower h_z, and the contours with a constant barrier height also decrease linearly with respect to $\omega_{\rm rf}$. Figure 4(b) compares h_z dependencies of the barrier height in this frequency range which all show a monotonic decrease with respect to h_z. Increasing $\omega_{\rm rf}$ shifts the h_z dependencies toward the negative h_z direction and makes the slope slightly steeper.

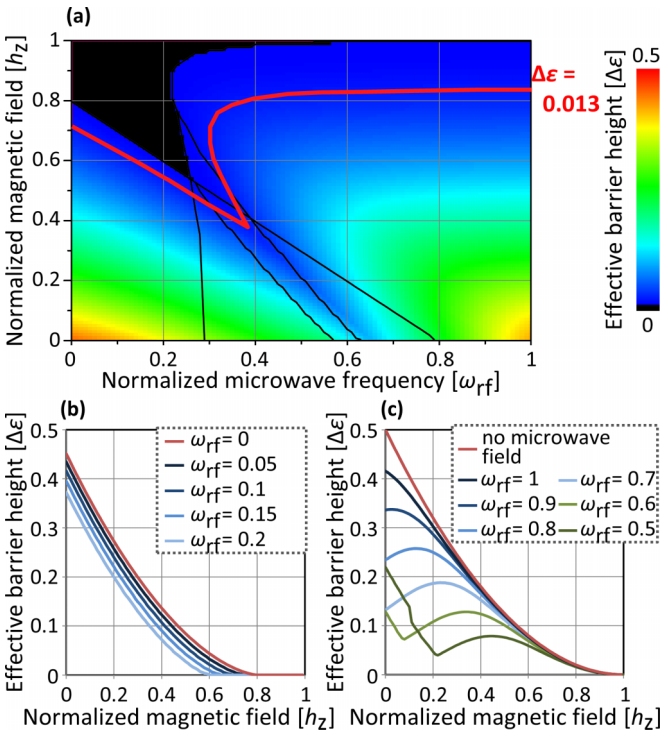

FIG. 4. (Color online) (a) Color map of barrier height calculated for $h_{\rm rf} = 0.05$. Black lines are boundaries between the phase portraits. The solid line denotes a contour of $\Delta\varepsilon = 0.013$. (b) and (c) Barrier heights for different values of $\omega_{\rm rf}$ plotted versus h_z.

Above the critical frequency, the value of h_z necessary for the deterministic switching suddenly increases, with only a small $(s|u)$ region existing near $h_z = 1$. This small $(s|u)$ region gradually vanishes as $\omega_{\rm rf}$ further increases. In addition, a trench in the barrier height protrudes from the tip of the $(s|u)$ region toward the lower right direction in the $(sr\,|sd|\,s)$ and $(sr\,|uad|\,s)$ regions. This trench is attributed to the two-step magnetization switching because such switching distributes the barrier height to two distinct transitions and consequently lowers the individual barrier heights. As $\omega_{\rm rf}$ increases further, the trench disappears and the h_z dependencies of the barrier height show a monotonic decrease again. Figure 4(c) compares the h_z dependencies in this frequency range and also shows the analogous curve for the case without a microwave field. Microwave fields above the critical frequency modify the barrier height considerably for $h_z < 0.7$. On the other hand, for $h_z > 0.7$, where the barrier height is low, the barrier heights change little and coincide with the barrier height without a microwave field, showing that this lower part of the barrier is not susceptible to microwave fields. The lower part is essential for studying fast magnetization switching, such as that in the writing process in recording applications. This is because the magnetic materials used in these applications have intrinsic $K_{\rm u}^{\rm eff}$ high enough to attain long-term thermal stability and the barrier height must be drastically reduced by means of a magnetic field, a spin-torque current, or other methods for magnetization switching to occur within the time required for device operation. As can be seen in Fig. 4(c), the application of microwave fields above the critical frequency has a negligible influence on the lower part of the barrier and might therefore not affect fast magnetization switching. This is consistent with the experimental result that a microwave-assisted switching field becomes almost the same as that without a microwave field when $f_{\rm rf}$ is higher than the critical frequency [15].

C. Macrospin simulations

To confirm the validity of the calculated barrier height, we performed macrospin simulation based on the following LLG equation without normalization: $d\mathbf{m}/dt = -\gamma(\mathbf{m} \times \mathbf{H}^{\rm eff}) + \alpha\mathbf{m} \times (d\mathbf{m}/dt)$. The effective anisotropy field is chosen to be $H_{\rm k}^{\rm eff} = 3600$ Oe, which yields an intrinsic FMR frequency of approximately 10 GHz and $K_{\rm u}^{\rm eff} = 1.08 \times 10^6\,{\rm erg/cm^3}$. The Gilbert damping constant α is set to 0.02. Thermal fluctuation at $T = 300$ K is taken into account through a random thermal field. The amplitude of the random thermal field is calculated from Eqs. (6) and (7) by assuming a cylindrical magnet with a diameter of 50 nm, a thickness of 5 nm, and a saturation magnetization of 600 emu/cm^3. The nonuniformity in the demagnetizing field of the shape is neglected.

We estimate the switching probability $P_{\rm sw}$ by calculating the time evolution of the magnetization motion over 100 ns and counting the switching events for 50 trials. The initial magnetization direction is the $+z$ direction. To be precise, the macrospin simulations and the barrier heights calculated from the effective energy treat magnetization switching differently. In the former, the magnetization evolves from the initial $+z$ direction, while in the latter, $\Delta\varepsilon$ is measured from the equilibrium magnetization state before switching. That is, the initial $+z$ direction in the macrospin simulations is slightly

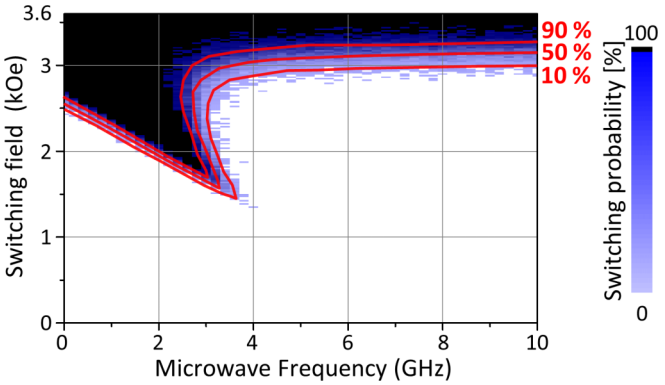

FIG. 5. (Color online) Color map of switching probability obtained from macrospin simulations. The solid lines denote the contours of 10%, 50%, and 90%. Because the effective anisotropy field $H_k^{\rm eff} = 3600$ Oe yields an intrinsic FMR frequency of approximately 10 GHz, the horizontal axis up to 10 GHz and the vertical axis up to 3.6 kOe are comparable to the axes in Fig. 4(a).

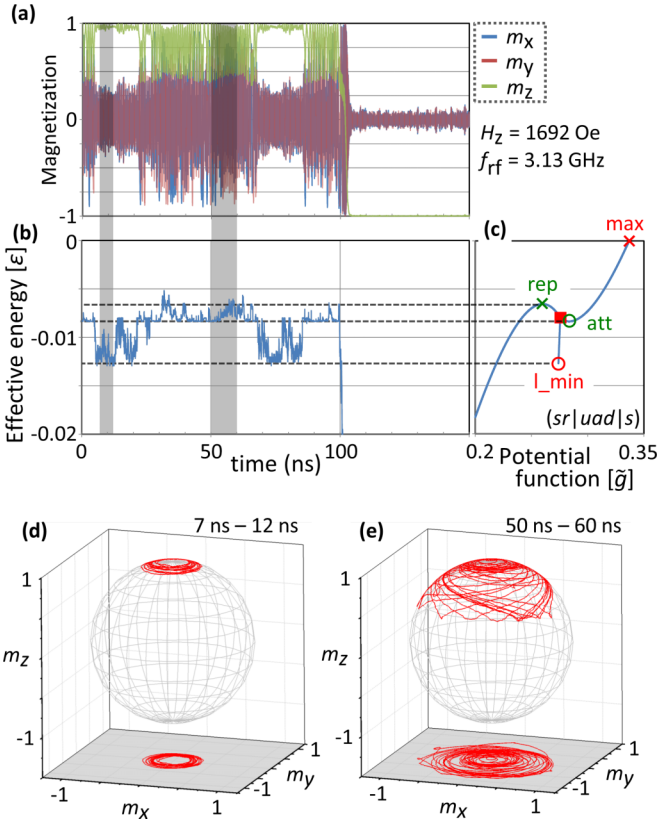

FIG. 6. (Color online) (a) Time evolution of x, y, z components of magnetization direction. (b) Corresponding time evolution of the effective energy ε. (c) Profile of ε that is classified into the $(sr\,|uad|\,s)$ phase portrait. (d) and (e) Trajectory of magnetization direction from 7 to 12 ns and from 50 to 60 ns, respectively. These time ranges are shown in (a) by shading.

excited compared to the equilibrium magnetization state before switching. In most cases, however, the increase in ε in the initial state is very small and has little influence on the switching probability. Figure 5 shows the results as a color map in the $f_{\rm rf}$-H_z plane. The microwave field amplitude is 180 Oe, making the ratio to the effective anisotropy field equivalent to that used to produce Fig. 4(a) ($H_{\rm rf}/H_k^{\rm eff} = 0.05$). The correspondence between the switching probability and barrier height is obvious, and the contour of $P_{\rm sw} = 10\%$ shows exact agreement with that of $\Delta\varepsilon = 0.013$ except in the $(sr\,|uad|\,s)$ region where only the higher value of the two barrier heights is plotted and the actual switching probability decreases because of the existence of the other transition. The agreement is considered qualitatively reasonable, as judged according to the Néel-Arrhenius law, $P_{\rm sw} = 1 - \exp[-t\,f_0 \exp(-\Delta E/K_{\rm B}T)]$ [23] where t is the simulation time. In this evaluation, a typical value of 10 GHz is used for the attempt frequency f_0.

Finally, we give one example of two-step magnetization switching. Figure 6(a) shows the time evolution of the magnetization direction calculated for $H_z = 1692$ Oe, and $f_{\rm rf} = 3.13$ GHz, which corresponds to the $(sr\,|uad|\,s)$ phase portrait. Before the magnetization switches to the $-z$ direction at around 100 ns, the magnetization clearly exhibits two kinds of motion: one kind appears from 5 to 20 ns and from 70 to 85 ns, and the second kind appears from 20 to 70 ns and from 85 ns until the switching occurs. In the first kind, the magnetization precesses around the $+z$ direction, as shown by the typical magnetization trajectory in Fig. 6(d). To understand this magnetization motion, we calculate the time evolution of ε and the corresponding ε profile [Figs 6(b) and 6(c)], which clearly shows that the first kind originates from the magnetization fluctuating around the local minimum point. This result is consistent with the magnetization motion [Fig. 6(d)] because the local minimum point corresponds to the magnetization rotation with a constant cone angle in synchronization with the microwave field. Analyzed from the viewpoint of ε, the second kind corresponds to the attractive limit cycle. The complex magnetization dynamics shown in Fig. 6(e) can therefore be understood as the quasiperiodic motion resulting from the attractive limit cycle in the rotating frame.

IV. CONCLUSIONS

We studied thermally activated magnetization switching for a uniaxial system in a microwave magnetic field. We derived an effective energy from the LLG equation formulated in the rotating frame that reflects both static and microwave magnetic fields, and classified switching paths according to the effective-energy profiles. Limit cycles as well as fixed points are found to affect the switching paths, and, under certain conditions, the switching becomes a two-step process. The results from the effective-energy approach agree with the previous studies, and the switching field for deterministic switching is predicted by the Stoner-Wohlfarth model that takes account of the fictitious field originating from the microwave field. Moreover, our approach provides the precise critical frequency because the critical frequency is given by the boundary above which limit cycles prevent switching. The barrier heights for thermally activated switching can also be calculated from the effective energy. Applying microwave fields below the critical frequency shifts the H_z dependencies of the barrier heights toward the lower H_z direction and makes the slope steeper. Applying microwave fields above the critical frequency modifies only the higher part of the barrier height

and affects the lower part very little, which means that fast magnetization switching is not susceptible to such microwave magnetic fields. The barrier height quantitatively explains the switching probability calculated from the macrospin simulations.

ACKNOWLEDGMENT

This work was partially supported by Strategic Promotion of Innovative Research and Development from Japan Science and Technology Agency (JST).

[1] C. Kittel, Phys. Rev. **71**, 270 (1947).
[2] S. V. Vonsovskii, *Ferromagnetic Resonance* (Pergamon, New York, 1966).
[3] C. Thirion, W. Wernsdorfer, and D. Mailly, Nat. Mater. **2**, 524 (2003).
[4] J.-G. Zhu, X. Zhu, and Y. Tang, IEEE Trans. Magn. **44**, 125 (2008).
[5] G. Winkler, D. Suess, J. Lee, J. Fidler, M. A. Bashir, J. Dean, A. Goncharov, G. Hrkac, S. Bance, and T. Schrefl, Appl. Phys. Lett. **94**, 232501 (2009).
[6] S. Li, B. Livshitz, H. N. Bertram, E. E. Fullerton, and V. Lomakin, J. Appl. Phys. **105**, 07B909 (2009).
[7] R. Sato, K. Mizushima, T. Nagasawa, and K. Kudo, Patent No. WO/2011/030449, 2011.
[8] T. Yang, H. Suto, T. Nagasawa, K. Kudo, K. Mizushima, and R. Sato, J. Appl. Phys. **114**, 213901 (2013).
[9] H. Suto, T. Nagasawa, K. Kudo, K. Mizushima, and R. Sato, Nanotechnology **25**, 245501 (2014).
[10] H. T. Nembach, P. M. Pimentel, S. J. Hermsdoerfer, B. Leven, B. Hillebrands, and S. O. Demokritov, Appl. Phys. Lett. **90**, 062503 (2007).
[11] Y. Nozaki, M. Ohta, S. Taharazako, K. Tateishi, S. Yoshimura, and K. Matsuyama, Appl. Phys. Lett. **91**, 082510 (2007).
[12] G. Woltersdorf and C. H. Back, Phys. Rev. Lett. **99**, 227207 (2007).
[13] T. Moriyama, R. Cao, J. Q. Xiao, J. Lu, X. R. Wang, Q. Wen, and H. W. Zhang, Appl. Phys. Lett. **90**, 152503 (2007).
[14] H. Suto, T. Nagasawa, K. Kudo, K. Mizushima, and R. Sato, Appl. Phys. Express **8**, 023001 (2015).
[15] S. Okamoto, N. Kikuchi, M. Furuta, O. Kitakami, and T. Shimatsu, Phys. Rev. Lett. **109**, 237209 (2012).
[16] G. Bertotti, C. Serpico, and I. D. Mayergoyz, Phys. Rev. Lett. **86**, 724 (2001).
[17] G. Bertotti, I. D. Mayergoyz, C. Serpico, M. d'Aquino, and R. Bonin, J. Appl. Phys. **105**, 07B712 (2009).
[18] T. Taniguchi, Phys. Rev. B **90**, 024424 (2014).
[19] J. C. Slonczewski, J. Magn. Magn. Mater. **159**, L1 (1996).
[20] L. Berger, Phys. Rev. B **54**, 9353 (1996).
[21] T. Taniguchi, Y. Utsumi, and H. Imamura, Phys. Rev. B **88**, 214414 (2013).
[22] W. F. Brown, Jr., Phys. Rev. **130**, 1677 (1963).
[23] L. Néel, Adv. Phys. **4**, 191 (1955).